Evaluating Expected Signal Loss due to SiPM Saturation for Short, Low Flux Light Pulses in Tapered Light Pipe Systems

J. Davies, *(Department of Physics, Imperial College London)*, D. Neely, *(Central Laser Facility, STFC Rutherford Appleton Laboratory)*, C. D. Armstrong, *(Department of Plasma Physics, University of Strathclyde; Central Laser Facility, STFC Rutherford Appleton Laboratory)*, September 2019

***Abstract*—Tapered light pipe systems connecting an arbitrary scintillator to a SiPM are simulated using a ray tracing program. A Monte Carlo method is used to estimate the signal losses in the system caused by both flux loss upon reflections, and from the response of an SiPM losing linearity in regions of higher flux density. Square, octagonal, and circular profiled tapered light pipes are modelled with various lengths and with the sloped walls having various reflective properties. In all simulated systems the loss due to partial saturation is found to be less than 1% for short and low intensity pulses when the incoming light is Lambertian and spatially uniform, varying only slightly from a system with uniform flux density over the detector surface.**

Smooth sided lights pipes wrapped in PTFE, rather than rough sided or silvered pipes; and, partially due to the geometric construction of the systems, square profiled pipes are generally seen to the most efficient. It is not seen that wrapping the exposed sides of the entrance window on the SiPM with PTFE has any noticeable effect on system efficiency as might be expected, this result being supported by geometric arguments.

I. Introduction

LIGHT pipes are solid transparent structures often used to channel photons generated inside a scintillating material onto a detection device. In recent years silicon photomultipliers (SiPMs) have come to replace photomultiplier tubes as the predominantly used low light detection device in high energy physics. [1]

A SiPM is formed from an array of microcells, each containing an independently acting avalanche photodiode. Upon absorbing a photon a microcell will release an electronic pulse, pulses from all of the cells are superimposed onto each other to form a linearly dependent output signal. After emitting a signal a diode will remain unresponsive during its recovery period whilst the voltage across the diode returns to its original value. Any photon incident on this microcell in this period will not produce a pulse and the linear response of the output sign to the incoming photon number is lost. [1]

For cases considering short pulses of light, where the pulse length is much shorter than the recovery time of a cell, each microcell can only be activated once per pulse.

In this report, partial saturation due to light pipe systems producing non-uniform illuminations across the surface of a SiPM and how this effects the output signal will be investigated for short light pulses. In these pulses the number of incoming photons will be much lower than the total number of microcells. Therefore, saturation would not be expected to be the dominant limiting factor in photon detection.

The effect will be investigated over multiple tapered light pipe (TLP) geometries and reflective properties of the sloped surfaces to determine if different designs had a major impact on the uniformity of the resultant illumination.

II. Simulation Design

The simulation created for this investigation is a python-based ray tracing program made to facilitate using a Monte Carlo approach to approximate the amount of photons lost due to saturation for various geometries of TLPs.

The system that rays propagated through was described by a collection of surfaces which represent the interfaces between different media, each surface being described as the solution of a particular equation and having a defined extent. Using this information the propagation cycle for each ray started with the ray calculating all possible future surface intercepts given its current position and direction, assuming unimpeded movement, and then advancing to the closest surface.

Once advanced to a surface the ray's direction would change according to the surface properties. In the investigation, four surface types were modelled:

- Rough glass surface wrapped in PTFE.
  - Acts as an ideal diffuse reflector, with the directional vector of reflected rays following Lambert's Cosine Law.
- Smooth glass with silvered surface.
  - Acts as an ideal specular reflector.
- Smooth, polished glass surface wrapped in PTFE.
  - Reflections are specular at incident angles greater then critical angle of interface, otherwise rays will immediately and diffusely reflects from PTFE wrapping.
- Boundary between transmissive media.
  - Rays refract or specularly reflect according to Snell's law.

A ray could only follow a single path and, in cases where transmission and reflection modes would be possible via Fresnel coefficients, a ray deterministically selected a mode based on the angle of incidence.

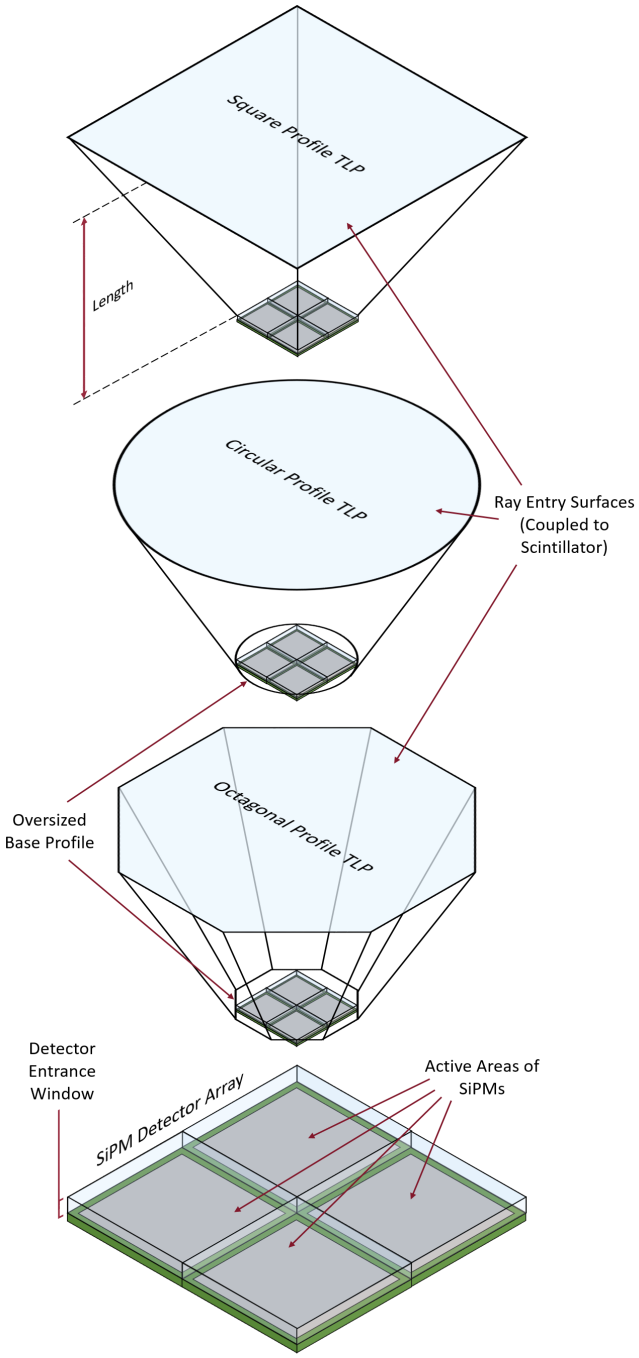

Fig. 1. Schematics of the three investigated tapered light pipe profiles and the SiPM detector array used to observe them. Various lengths, measured between the two parallel faces of the tapered prism, were also investigated while keeping the entry surface area constant, thus changing the angle of the sloped face. The entry (top) surface of each system is coupled to a scintillator that acts as a Lambertian light source, with uniform spacial flux density over the surface. It can be seen here how the exiting surface of non-square pipes were oversized to encompass the detectors entrance window. The bottom schematic is of a 2×2 array of KETEK PM3325-WB-D0 SiPMs that was simulated and used to detect the out-coming light. (SiPM schematic adapted from [4])

For PTFE, the refractive index was taken as 1.35 and the reflectivity as 0.95, which are values for 430 nm wavelength light. The latter value was also used as the reflection and transmission coefficient for all surfaces in the simulation. Upon each reflection the ray had a chance of not being terminated equal to the reflectivity of the surface. If a ray had not been terminated after being propagated to a surface, then the propagation cycle would return to the beginning with the ray searching for new intercepts. [2][3]

The whole of the face of the detector was modelled as black and would terminate any incident rays, if the ray hit the active area of the detector then the corresponding pixel would increase the count of incident rays by one.

The detector was modelled as a 2×2 array of KETEK PM3325-WB-D0 SiPMs, each with an active area 3 mm across with an oversized 0.4 mm thick glass entrance window, 3.315 mm across with a refractive index of 1.52. The active area of each SiPM was approximated as being a uniform square 118×118 grid of mircocells, with a fill factor of 1. [4]

III. Tapered Light Pipe Investigation

In order to investigate the performance of various TLPs, a model of an arbitrary scintillator was created and coupled to the light pipes. In this model scintillator, rays entered the light pipes with a uniform spacial distribution across a 625 mm^2 entry plane, with a Lambertian directional distribution across a 2π sr solid angle with rays projecting toward the detector. A ray that later reflected back onto the entry plane is assumed to preform four reflections before returning to another random point on the plane with a new random direction.

This entry plane formed the top of the TLP, which consisted of a tapered prism made from silica glass with a refractive index of 1.46. The prism tapers down such that the perimeter of the smaller face entirely encompassed the 6.63 mm square detector entrance window. Schematics of these tapered prisms are shown in Fig. 1, here it can be seen how the bottom face of non-square systems were oversized to match the detector entrance window. TLPs with square, circular, and octagonal profiles were all tested with lengths of 20 mm, 40mm, 60 mm, and 80mm. [5]

The smallest face of the TPL, at the base facing the detector, was always modelled as being smooth and wrapped in PTFE, leaving a square hole for the detector. The sides of the detector entrance window were also modelled as being smooth glass. Tests were done both with and without the sides of the detector window having a PTFE wrapping. The detector was tested both in contact with, and small separations from the TLPs.

The sloped walls of the TLPs were modelled as being a smooth silvered surface, a smooth glass surface with PTFE wrapping, or rough glass surface with PTFE wrapping.

A. Estimation of Partial Saturation Effect for 1000 Instantaneously Absorbed Photons

The detector has a total of 55696 microcells. In each trail, rays entered and propagated through a system until 1000 rays have landed on the active area of the detector. The investigation

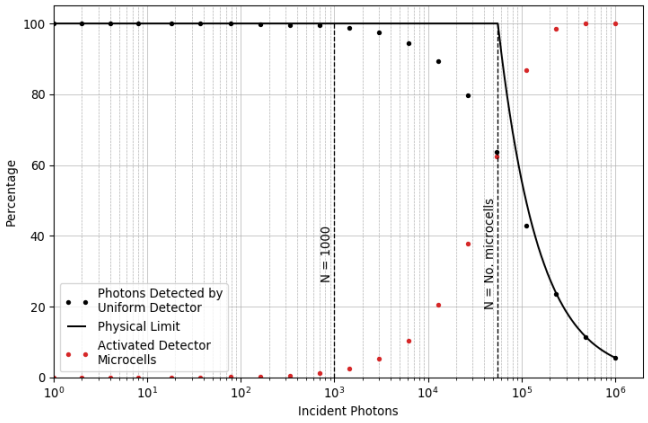

Fig. 2. Percentage of photons incident on a uniformly illuminated SiPM with 55696 microcells in a short light pulse that are expected to activate a microcell, where the only limitation to this is that throughout a light pulse an increasing number of microcells become activated and therefore unavailable for further activity within that pulse due to the pulse length being much shorter than the recovery time of any given microcell. The physical upper limit to the percentage of activating photons is also shown, along with the percentage of microcells that are expected to be activated. It can be seen here how, for the low flux pulses investigated in this report (N = 1000), these losses are almost negligible. The illumination on the SiPM shown here is perfectly uniform, however all systems simulated in this report closely followed the relationship shown.

was done in this way to ensure that the sample of rays on the detector surface was a constant size, so that the effect of Monte Carlo noise was comparable between trails as this was found to be a much stronger non-uniformity effect than varying system geometry.

Each detector microcell kept a count of the number of incident photons on it throughout each trail. The linearity efficiency is the percentage of the rays, that had already reached the detector's active area, to activate a microcell when the only effect that could prevent this would be the microcell already being in saturation. This was calculated at the end of each trail by

$$eff_{lin} = \left(1 - \frac{\sum_{P_i \neq 0}(P_i - 1)}{1000}\right) \times 100\%, \qquad (1)$$

where P_i is the population of detector microcell i.

The exiting efficiency of the TLP is the percentage of light entring the TLP that reached the detector's active area and was calculated at the end of each trail by

$$eff_{exit} = \frac{1000}{N_{trail}} \times 100\%, \qquad (2)$$

where N_{trail} is the number of input photons used to achieve 1000 photons reaching the detector face.

The resultant efficiency of the system is

$$eff_{system} = \frac{eff_{lin} \times eff_{exit}}{100}, \qquad (3)$$

and is the percentage of light entering the TLP system that is expected to be measured by the SiPMs.

B. Comparison to Partial Saturation Effect for Uniform Case

For comparison, the performance of a perfectly uniform system was estimated by forming a 55696 cell grid of counters set to zero. Then counters were chosen at random (allowing for repeats) and incremented by one until the sum across the whole grid equalled the required number of incident photons. The linearity efficiency could then be calculated using (1).

IV. Performance of Various Systems

Summaries of the performances of the various investigated systems are tabulated in the Appendix with uncertainties (σ) reported as the standard error on the mean of an observed value over $\sim$ 200 trails.

A. Effect of Flux Uniformity

The perfectly uniform detector model produced an eff_{lin} of 99.12% and none of the simulated light pipes differed from this by more than an absolute value of 0.08%, which is lower than the natural variation of eff_{lin} between trails in any of the simulated systems. It can therefore be concluded that the partial saturation and the non-linearity caused by it is insignificant at this level of incoming flux, when considering the incoming flux as being spatially and directionally uniform. Therefore the non-linearity effect and can be reasonably ignored and instead eff_{exit} should be viewed as the limiting factor.

However, at this low level of incoming flux a realistic scintillator might be expected to only be responding to a few ionising particles within each light pulse, therefore light would enter the TLP from a heavily localised sources. Additional but limited tests were done where every ray in a single trail entered the light pipe from the same random point on the entry plane, in order to simulate an extreme case of light source non-uniformity. These tests were done on TLP systems with the three different previously described reflective treatments of the sloped walls, lengths of 20 mm and 40 mm, using wrapping around the detector window, and a detector separation of 0 mm. The number of photons reaching the detector in the pulse was kept at 1000. For all but one these 18 systems, the observed value of eff_{lin} was within 2σ of the value found when the incoming light was spatially uniform, and was generally higher. This is not enough evidence to suggest that changing the spacial distribution of incoming light had any effect on eff_{lin}.

These additional limited tests do not allow for a scintillation event to emit radiation non-isotropically. However, to account for this the type of expected events would need to be specified in greater detail. These tests also still use a model of a scintillator that randomises a ray's position and direction upon incidence on the surface between the scintillator and TLP. This effect will nullify the effect of a light source's spacial non-uniformity for many of the rays, and while it may be partially accurate it should be improved upon if the system is to be used to investigate non-uniform sources. Further investigation into the effects of non-uniform light sources is beyond the scope of this report.

In Fig. 2 the projected performance of a perfectly uniform detector is shown in comparison the physical limit of performance. The simulated systems were seen not to deviate from the performance of the uniform detector by more than a few percentage across the range shown. For incident photon

numbers much greater than the total numbers of microcells it can be seen that the uniform performance approach the physical limit, given by

$$eff_{lin}^{limit} = 100\% \times \begin{cases} 1, & \text{if } N_p \leq N_m \\ \dfrac{N_m}{N_p}, & \text{otherwise} \end{cases} \quad (4)$$

where N_p is the number of photons in a short pulse and N_m is the number of detector microcells. Approaching the physical limit shows that the detector is reaching saturation, as can also be seen from Fig. 2 in the percentage of activated microcells.

B. Exiting Efficiency of Various TLPs

The eff_{exit} values for square profile systems were consistently higher than for circular or octagonal systems when considering using the PTFE wrapping, especially with a smooth glass surface. This will in part be due to the geometry being optimized for square profiles due to the requirement that the base of the TLP must completely encompass the square-shaped detector entrance window, thus leaving to flat surfaces facing away form the detector in the case of non-square profiles as seen in Fig. 1. Downsizing the base of the TLP would increase eff_{exit}, nominally at the cost of eff_{lin} due to the illumination being more localised at the center of the detector. However, as previously stated, the effect of eff_{lin} can mostly be ignored.

Using a rough surface, rather than a smooth surface, wrapped in PTFE caused a 14.7% to 47.3% relative decrease in eff_{exit} for square systems and a 3.3% to 40.0% relative decrease in eff_{exit} for octagonal systems. Using a rough surface was only shown to have a benefit for circular profiles.

Introducing a circular profile or specular coating lowered eff_{exit} in every case other than when they are both used, in which they were shown to work together well.

Separating the detector and light pipe a distance of 0.25 mm was only ever seen to reduce eff_{exit}.

It was seen throughout that shorter TLPs were favourable as they produced higher eff_{exit} values. This is partially because it would take less random reflections to traverses their length but also because from any point on the entry plane the detector surface occupies a larger solid angle. However, the latter effect is not completely dominant as when TLP length is increased, eff_{exit} decreases at a rate slower than the average solid angle of the detector over all points on the entry plane. [6]

C. Effect of Wrapping the Detector Entrance Window

At no point in the investigation was it seen that wrapping PTFE around the sides of the detector entrance window significantly increased eff_{exit}. This result is supported by the fact that it can be shown geometrically that for all of the TLP profiles and lengths investigated, it was impossible for a ray starting on the entry plane to hit a side of the detector window at an incident angle lower than the critical angle between the detector glass and the surrounding air (41°), without reflecting off a wall of the TLP first. Thus, the internally reflecting properties of the entrance window would contain these rays and specularly reflect them onto the detector face.

When using the profiles and entry plane size that was used in this investigation, this direct transmission from entry plane through the side of the detector entrance window is forbidden for TLP lengths down to 14.4 mm. It is therefore reasonable to assume that most rays leaving a sufficiently long TLP will also be contained by the reflective properties of the side of the entrance window, even without PTFE wrapping.

The model used in this report does not account for the partial transmission and reflection that occurs at a dielectric boundary, in reality there would be leakage from any ray internally reflecting from the inside of the unwrapped detector window. An improved model that did account for this could lead to distinction between the efficiency of wrapped and unwrapped detector systems.

REFERENCES

[1] "Introduction to the silicon photomultiplier AND9770/D," ON Semiconductor, July 2018.

[2] R. H. French, J. M. Rodrguez-Parada *et al.*, "Optical properties of materials for concentrator photovoltaic systems," in *2009 34th IEEE Photovoltaic Specialists Conference (PVSC)*, June 2009, pp. 000 394–000 399.

[3] M. Janecek, "Reflectivity spectra for commonly used reflectors," *IEEE Transactions on Nuclear Science*, vol. 59, no. 3, pp. 490–497, June 2012.

[4] "SiPM product data sheet - PM3325-WB-D0," KETEK GmbH, June 2019.

[5] R. Kitamura, L. Pilon, and M. Jonasz, "Optical constants of silica glass from extreme ultraviolet to far infrared at near room temperature," *Applied Optics*, vol. 46, no. 33, pp. 8118–8133, Nov 2007. [Online]. Available: ao.osa.org/abstract.cfm?URI=ao-46-33-8118

[6] R. J. Mathar, "Solid angle of a rectangular plate," *Max-Planck Institute of Astronomy*, March 2019. [Online]. Available: mpia.de/ mathar/public/mathar20051002.pdf

APPENDIX

TABLE I
PERFORMANCE OF SMOOTH SIDED, PTFE WRAPPED TLPS

Profile	Length (mm)	Detector Seperation (mm)	Wrapping Around Detector				No Wrapping Around Detector			
			Exiting Efficiency (%)	σ	Linearity Efficiency (%)	σ	Exiting Efficiency (%)	σ	Linearity Efficiency (%)	σ
Square	20	0	21.55	0.04	99.09	0.02	21.59	0.05	99.11	0.02
		0.25	10.77	0.02	99.09	0.02	10.78	0.02	99.12	0.02
	40	0	17.12	0.03	99.08	0.02	17.02	0.04	99.04	0.02
		0.25	12.87	0.03	99.11	0.02	12.89	0.03	99.07	0.02
	60	0	13.45	0.03	99.09	0.02	13.43	0.03	99.11	0.02
		0.25	10.96	0.02	99.15	0.02	10.97	0.02	99.12	0.02
	80	0	11.79	0.02	99.11	0.02	11.73	0.02	99.08	0.02
		0.25	10.00	0.02	99.11	0.02	9.99	0.02	99.07	0.02
Circular	20	0	11.91	0.03	99.11	0.02	11.97	0.02	99.09	0.02
		0.25	6.75	0.01	99.11	0.02	6.73	0.01	99.11	0.02
	40	0	6.95	0.01	99.08	0.02	6.96	0.01	99.10	0.02
		0.25	5.02	0.01	99.10	0.02	5.00	0.01	99.10	0.02
	60	0	4.82	0.01	99.08	0.02	4.86	0.01	99.09	0.02
		0.25	3.64	0.01	99.14	0.02	3.65	0.01	99.10	0.02
	80	0	3.96	0.01	99.08	0.02	3.98	0.01	99.04	0.02
		0.25	3.07	0.01	99.10	0.02	3.07	0.01	99.07	0.02
Octagonal	20	0	16.41	0.03	99.09	0.02	16.48	0.03	99.11	0.02
		0.25	8.43	0.02	99.10	0.02	8.47	0.02	99.06	0.02
	40	0	13.24	0.03	99.09	0.02	13.34	0.03	99.11	0.02
		0.25	9.00	0.02	99.06	0.02	9.01	0.02	99.10	0.02
	60	0	10.82	0.02	99.07	0.02	10.84	0.02	99.09	0.02
		0.25	7.87	0.02	99.05	0.02	7.86	0.02	99.10	0.02
	80	0	9.58	0.02	99.09	0.02	9.64	0.02	99.08	0.02
		0.25	7.27	0.02	99.06	0.02	7.25	0.02	99.12	0.02

TABLE II
PERFORMANCE OF ROUGH SIDED, PTFE WRAPPED TLPS

PTFE Wrapped Rough Surface										
Profile	Length (mm)	Detector Seperation (mm)	Wrapping Around Detector				No Wrapping Around Detector			
			Exiting Efficiency (%)	σ	Linearity Efficiency (%)	σ	Exiting Efficiency (%)	σ	Linearity Efficiency (%)	σ
Square	20	0	18.43	0.04	99.10	0.02	18.41	0.04	99.11	0.02
		0.25	10.34	0.02	99.05	0.02	10.30	0.02	99.08	0.02
	40	0	12.71	0.02	99.09	0.02	12.67	0.03	99.07	0.02
		0.25	9.46	0.02	99.07	0.02	9.39	0.02	99.06	0.02
	60	0	8.80	0.02	99.11	0.02	8.78	0.02	99.12	0.02
		0.25	6.89	0.02	99.11	0.02	6.89	0.02	99.09	0.02
	80	0	6.21	0.01	99.09	0.02	6.18	0.01	99.11	0.02
		0.25	5.00	0.01	99.11	0.02	4.99	0.01	99.13	0.02
Circular	20	0	16.21	0.03	99.13	0.02	16.18	0.04	99.12	0.02
		0.25	8.58	0.02	99.09	0.02	8.52	0.02	99.07	0.02
	40	0	11.98	0.02	99.09	0.02	11.94	0.02	99.11	0.02
		0.25	7.99	0.02	99.08	0.02	7.99	0.02	99.10	0.02
	60	0	8.69	0.02	99.08	0.02	8.70	0.02	99.11	0.02
		0.25	6.13	0.01	99.07	0.02	6.10	0.01	99.08	0.02
	80	0	6.35	0.01	99.12	0.02	6.35	0.01	99.11	0.02
		0.25	4.62	0.01	99.10	0.02	4.62	0.01	99.13	0.02
Octagonal	20	0	15.86	0.03	99.13	0.02	15.87	0.03	99.15	0.02
		0.25	8.31	0.02	99.12	0.02	8.29	0.02	99.10	0.02
	40	0	11.81	0.03	99.09	0.02	11.77	0.02	99.06	0.02
		0.25	7.77	0.02	99.08	0.02	7.75	0.02	99.08	0.02
	60	0	8.58	0.02	99.11	0.02	8.55	0.02	99.08	0.02
		0.25	5.99	0.01	99.15	0.02	5.98	0.01	99.12	0.02
	80	0	6.33	0.01	99.14	0.02	6.30	0.01	99.11	0.02
		0.25	4.54	0.01	99.10	0.02	4.54	0.01	99.15	0.02

TABLE III
PERFORMANCE OF SPECULARLY COATED TLPS

Profile	Length (mm)	Detector Seperation (mm)	Wrapping Around Detector				No Wrapping Around Detector			
			Exiting Efficiency (%)	σ	Linearity Efficiency (%)	σ	Exiting Efficiency (%)	σ	Linearity Efficiency (%)	σ
Square	20	0	9.69	0.02	99.13	0.02	9.65	0.02	99.11	0.02
		0.25	4.48	0.01	99.13	0.02	4.46	0.01	99.10	0.02
	40	0	7.70	0.02	99.12	0.02	7.67	0.02	99.09	0.02
		0.25	3.47	0.01	99.09	0.02	3.46	0.01	99.11	0.02
	60	0	6.45	0.01	99.11	0.02	6.42	0.01	99.13	0.02
		0.25	2.94	0.01	99.08	0.02	2.94	0.01	99.12	0.02
	80	0	5.56	0.01	99.11	0.02	5.55	0.01	99.10	0.02
		0.25	2.58	0.01	99.12	0.02	2.58	0.01	99.10	0.02
Circular	20	0	9.79	0.02	99.11	0.02	9.75	0.02	99.11	0.02
		0.25	4.48	0.01	99.14	0.02	4.48	0.01	99.10	0.02
	40	0	7.94	0.02	99.11	0.02	7.98	0.02	99.14	0.02
		0.25	3.56	0.01	99.11	0.02	3.57	0.01	99.11	0.02
	60	0	6.83	0.02	99.11	0.02	6.81	0.01	99.14	0.02
		0.25	3.07	0.01	99.11	0.02	3.07	0.01	99.09	0.02
	80	0	5.93	0.01	99.14	0.02	5.95	0.01	99.13	0.02
		0.25	2.72	0.01	99.11	0.02	2.71	0.01	99.08	0.02
Octagonal	20	0	9.71	0.02	99.13	0.02	9.74	0.02	99.08	0.02
		0.25	4.46	0.01	99.12	0.02	4.46	0.01	99.10	0.02
	40	0	7.82	0.02	99.10	0.02	7.82	0.02	99.10	0.02
		0.25	3.54	0.01	99.14	0.02	3.52	0.01	99.12	0.02
	60	0	6.63	0.01	99.13	0.02	6.63	0.01	99.13	0.02
		0.25	3.00	0.01	99.09	0.02	3.00	0.01	99.12	0.02
	80	0	5.74	0.01	99.10	0.02	5.78	0.01	99.14	0.02
		0.25	2.65	0.01	99.08	0.02	2.63	0.01	99.09	0.02